Supporting Information

Engineering Fibrous-Interconnected Potassium bis(dioxovanadium) Phosphate Frameworks for Fast-Charging and High-Rate Sodium-Ion Supercapacitors

Ramu Manikandan,[a] C. Justin Raj,[b] Hyun Jung,[c] John D Rodney,[d,e] Periyasamy Sivakumar,[c] Rajavel Velayutham,[d] Amol Marotrao Kale,[d] S. Saranya,[f] Byung Chul Kim,[d] Jae-Min Oh[a]*

[a]*Department of Energy and Materials Engineering, Dongguk University-Seoul, Seoul 04620, Republic of Korea.*

[b]*Department of Physics, School of Advanced Sciences, Vellore Institute of Technology (VIT), Chennai Campus, Chennai, 600 127, Tamil Nadu, India.*

[c]*Advanced Functional Nanohybrid Material Laboratory, Department of Chemistry, Dongguk University Seoul-Campus, Jung-gu, Seoul, 04620, Republic of Korea*

[d]*Department of Advanced Components and Materials Engineering, Sunchon National University, 255, Jungang-ro, Suncheon-si, Jellanamdo, 57922, Republic of Korea*

[e]*Department of Physics, Saveetha School of Engineering, Saveetha Institute of Medical and Technical Sciences, Chennai 602105, Tamil Nadu, India.*

[f]*Department of Physics, Velammal college of Engineering and Technology, Velammal Village, Ring Road, Madurai, Tamil Nadu, India.*

E-mail: jmoh.nbml@gmail.com

1. Chemicals

Chemicals such as vanadium (IV) oxy sulfate hydrate ($VOSO_4 \cdot H_2O$), potassium persulfate ($K_2S_2O_8$), sodium hypophosphite (NaH_2PO_2), concentrated nitric acid (HNO_3), sodium perchlorate ($NaClO_4$) and acetonitrile (CH_3CN) were purchased from Sigma-Aldrich. All the chemical substances were analytically pure grade and used without additional purification.

2. Structural characterization

The structural aspects of the flexible carbon fiber cloth (C), synthesized KVOH-C, 2KVOP-C, 4KVOP-C and 6KVOP-C samples were analyzed by X-ray diffractometer (Ultima IV, Rigaku, Tokyo, Japan) using Cu Kα1 radiation (λ=1.5405 Å) at 50 kV and 40 mA in the range of 2θ = 5-90° with a period of 0.02° and a scan speed of 2°/min. Scanning electron microscopy (SEM, JEOL-7100F, Tokyo, Japan) was used to examine the surface morphology of the KVOH-C, 2KVOP-C, 4KVOP-C and 6KVOP-C samples at a 15 kV acceleration voltage. The X-ray photoelectron spectroscopy (XPS) measurements of KVOH-C and 4KVOP-C samples were studied using the Versaprobe II spectrometer, and the pattern was collected using Al Kα radiation. The Transmission electron microscopy (TEM) characterization of KVOH-C and 4KVOP-C samples was performed by immersing the electrode's active material region (1 × 1 cm^2) and dispersing it in isopropyl alcohol under sonication. The suspension solution was used for the morphological examination. High-resolution transmission electron microscope (HR-TEM) images for the fabricated samples were studied by JEOL model JEM- 2100F (Japan) at an accelerating voltage of 200 kV.

3. Fabrication of a symmetric device for sodium ion supercapacitor (SIS)

A Biologic Electrochemical Workstation (VMP3, France) was used to inspect the electrochemical characteristics of the sodium ion supercapacitor (SIS) at room temperature (~25 °C). The electrochemical parameters of the KVOH-C, 2KVOP-C, 4KVOP-C and 6KVOP-C electrodes

were thoroughly investigated in a conventional three-electrode system, with the as-synthesized samples serving as the working electrode, a platinum spring as the counter electrode and Ag/AgCl as the reference electrode in 1 M $NaClO_4$/acetonitrile (Na^+/ACN) electrolyte. The SIS was assembled using a stainless-steel split test cell (EQ-STC) from MTI Korea Ltd. The SIS was fabricated with a pair of 4KVOP-C as a positive and negative electrode of nearly equal weight and placed face-to-face by sandwiching a filter paper containing a Na^+/ACN electrolyte solution. The electrochemical measurements, such as cyclic voltammetry (CV), galvanostatic charge-discharge (GCD), and electrochemical impedance spectroscopy (EIS), were carried out in Na^+/ACN electrolyte. CV was studied for different scan rates from 5 to 100 mV s^{-1} and the GCD test was tested for various current densities, 4 to 25 mA cm^{-2}. Electrochemical impedance spectroscopy (EIS) was examined in the 0.01 Hz - 100 kHz frequency range at 0 V bias condition of 10 mV sinus amplitude.

The areal capacitance (A_{cap} in mF cm^{-2}) of the electrode were determined according to Equations (1) from GCD curves.

$$A_{cap} = \left(\frac{I \times \Delta t}{A \times \Delta V}\right) \quad (1)$$

Where, I is the discharge current (mA), Δt is the discharge time (s), A is the area (1×1 cm^2) of active material on carbon cloth (cm^2), and ΔV is the potential window (V).

The capacitance (C (ω)) can be defined as the mixture of the imaginary part of the capacitance (C" (ω)) and the real part of the capacitance (C' (ω)) and can be expressed as Equations (2).

$$C = \frac{-1}{(\omega Z'')} \quad (2)$$

Thus, the complex form of capacitance can be also written as:

$$C = C^{'}(\omega) - jC"(\omega) \quad (3)$$

The real and imaginary parts of the capacitance of the electrodes were determined according to the following Equations (4) and (5)

$$C' = \frac{Z"(\omega)}{\omega|Z(\omega)|^2} \quad (4)$$

$$C" = \frac{Z'(\omega)}{\omega|Z(\omega)|^2} \quad (5)$$

where ω is the angular frequency ($2\pi f_0$), Z' and Z" represent the real and imaginary parts of impedance, and $|Z(\omega)|$ is the modulus of impedance.

The areal capacitance (A_{cap} in mF cm^{-2}) value of the SIS were determined from the GCD curves using Equations (6),

$$C_G = \left(\frac{I \times \Delta t}{A \times \Delta V}\right) \quad (6)$$

Where, I is the discharge current (mA), Δt is the discharge time (s), A is the area (1×1 cm^2) of grown active material on carbon cloth (cm^2), and ΔV is the potential window (V).

The energy density (E_D) and power density (P_D) of SIS were calculated using Equations (7) and (8),

$$E_D = \frac{0.5A_{cap} \times \Delta V^2}{3.6} \quad (7)$$

$$P_D = \frac{E_D \times 3600}{\Delta t} \quad (8)$$

Where E_D is the energy density (Wh kg^{-1}), P_D is the power density (W kg^{-1}), A_{cap} is the areal capacitance of SIS, and Δt is the discharge time (s).

Computational details

Section. 4

For K-V_2O_5 1.6H_2O

At Temperature = 0 K and Smoothing sigma = 0 pts

$DOS_{(E_F)} = 20.58\ states/eV$

$C_{Q(E_F)} = 5.28 \times 10^{-37}\ F/eV$

$C_{Q(max)} = 3.05 \times 10^{-36}\ F/eV$

At Temperature = 296 K and Smoothing sigma = 0 pts

$DOS_{(E_F)} = 1129.95\ states/eV$

$C_{Q(E_F)} = 2.90 \times 10^{-35}\ F/eV$

$C_{Q(max)} = 1.31 \times 10^{-34}\ F/eV$

At Temperature = 296 K and Smoothing sigma = 3 pts

$DOS_{(E_F)} = 1072.78\ states/eV$

$C_{Q(E_F)} = 2.75 \times 10^{-35}\ F/eV$

$C_{Q(max)} = 1.08 \times 10^{-34}\ F/eV$

$Potential\ window = [-1.0, 1.0]\ eV\ (relative\ to\ E_F)$

$Average\ C_Q\ in\ window = 1.64 \times 10^{-35}\ F/eV$

For $K(VO_2)_2PO_4$

At Temperature = 0 K and Smoothing sigma = 0 pts

$DOS_{(E_F)} = 75.47\ states/eV$

$C_{Q(E_F)} = 1.93 \times 10^{-36}\ F/eV$

$C_{Q(max)} = 5.54 \times 10^{-36}\ F/eV$

At Temperature = 296 K and Smoothing sigma = 0 pts

$DOS_{(E_F)} = 3564.15\ states/eV$

$C_{Q(E_F)} = 9.14 \times 10^{-35}\ F/eV$

$C_{Q(max)} = 2.86 \times 10^{-34}\ F/eV$

At Temperature = 296 K and Smoothing sigma = 3 pts

$DOS_{(E_F)} = 3105.36\ states/eV$

$C_{Q(E_F)} = 7.97 \times 10^{-35}\ F/eV$

$C_{Q(max)} = 2.75 \times 10^{-34}\ F/eV$

$Potential\ window = [-1.0, 1.0]\ eV\ (relative\ to\ E_F)$

$Average\ C_Q\ in\ window = 4.66 \times 10^{-35}\ F/eV$

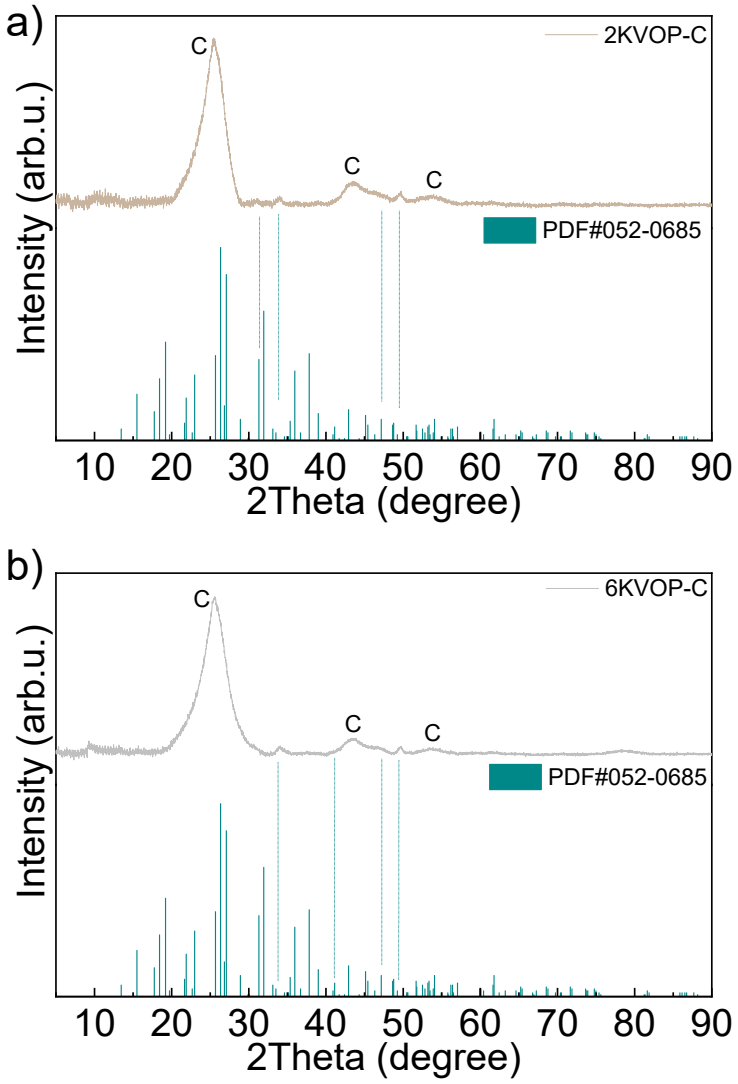

Figure. S1 XRD patterns of a) 2KVOP-C and b) 6KVOP-V samples.

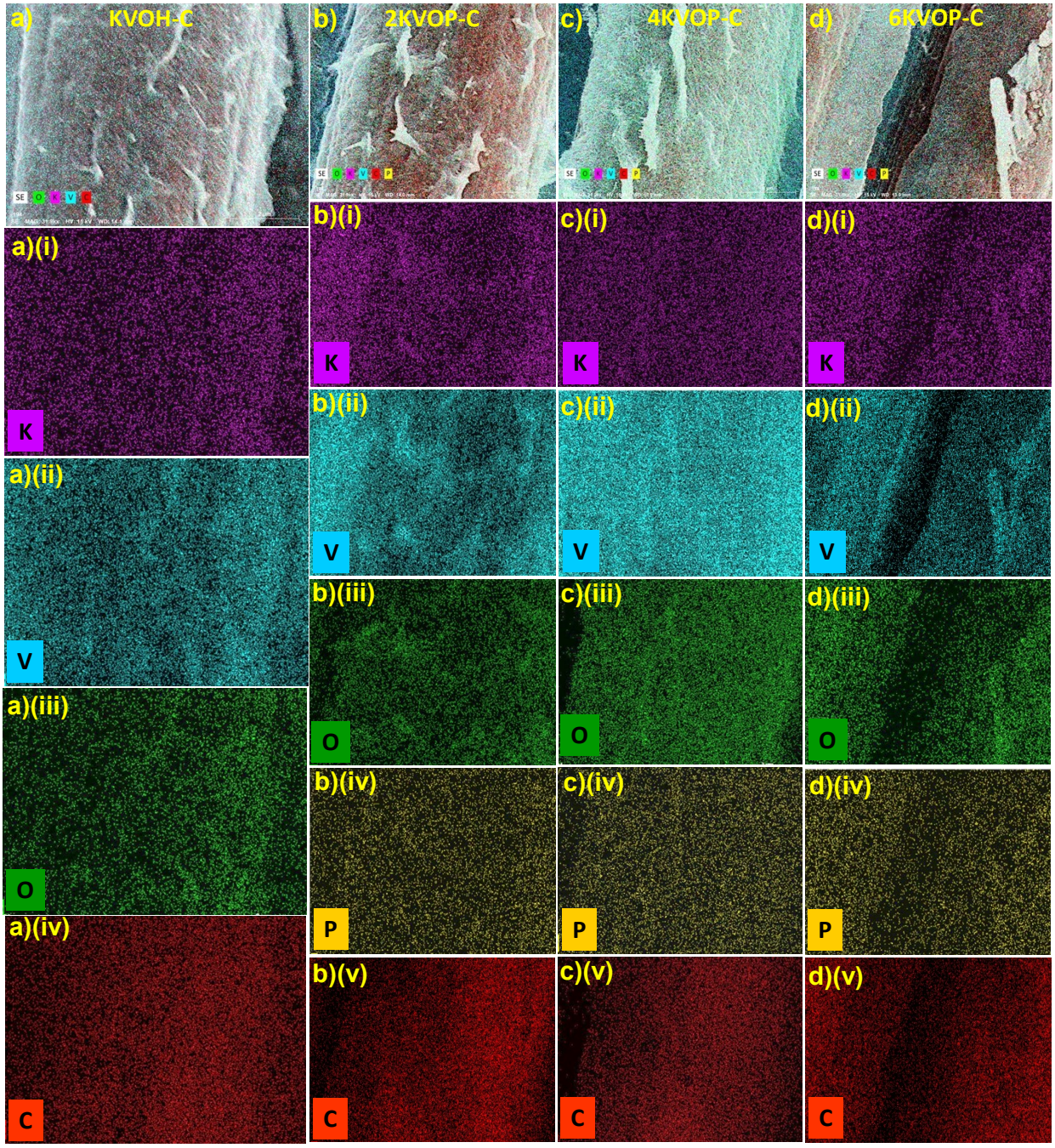

Figure. S2 FESEM EDS mapping images of (a)(i-iv) KVOH-C, (b)(i-v) 2KVOP-C, (c)(i-v) 4KVOP-C, and (d)(i-v) 6KVOP-C samples.

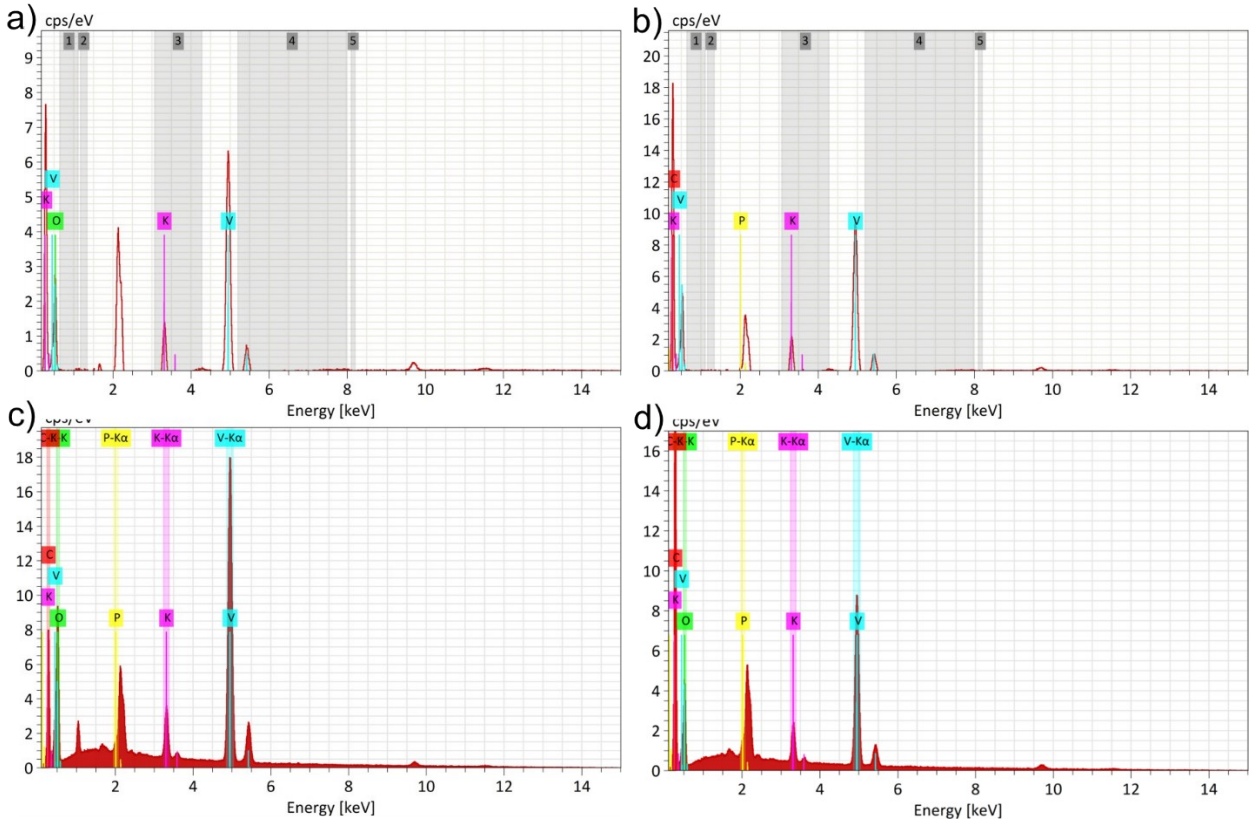

Figure. S3 FESEM EDS line spectrum of (a) KVOH-C, (b) 2KVOP-C, (c) 4KVOP-C, and (d) 6KVOP-C samples.

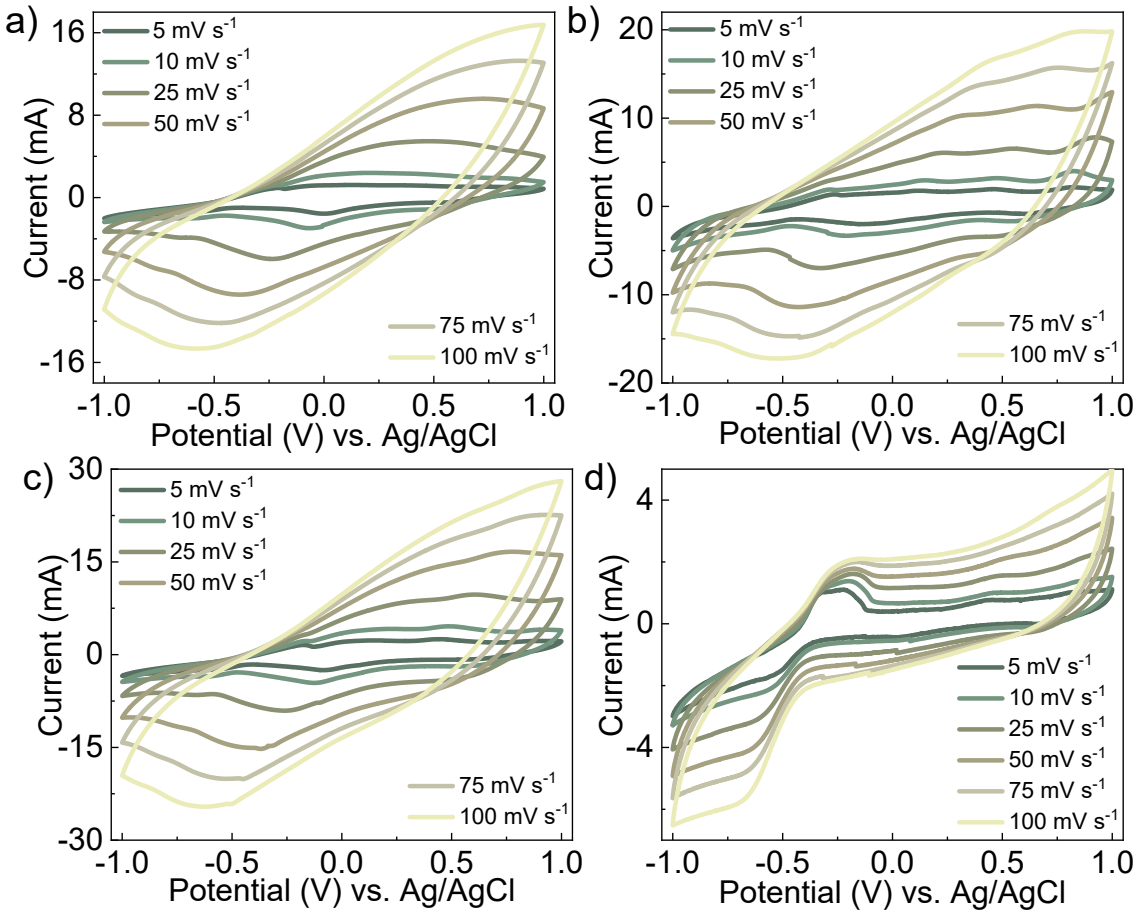

Figure. S4 CV curves of (a) KVOH-C, (b) 2KVOP-C, (c) 4KVOP-C, and (d) 6KVOP-C samples for various sweep rates (5, 10, 25, 50, 75 and 100 mV s^{-1}).

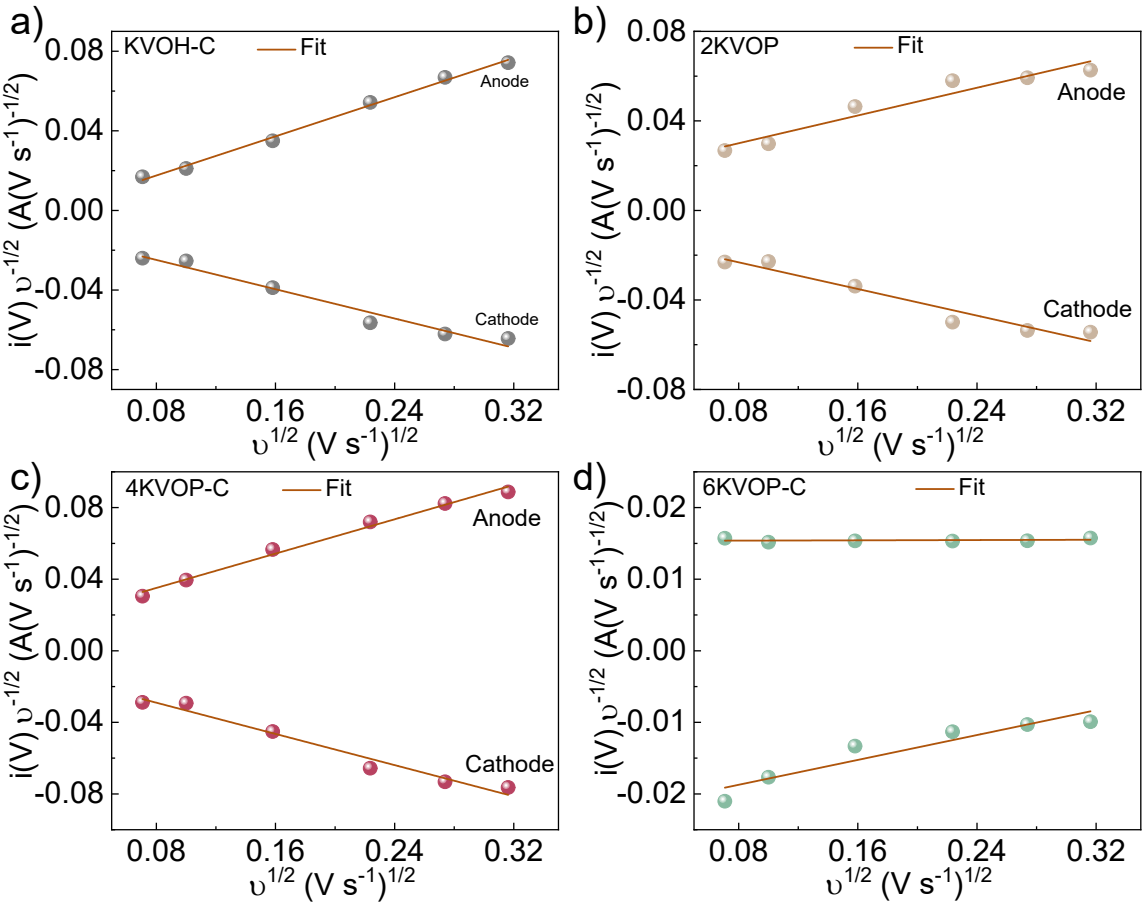

Figure. S5 Linear plot between $\upsilon^{1/2}$ vs $i\upsilon^{-1/2}$ for KVOH-C, 2KVOP-C, 4KVOP-C, and 6KVOP-C electrodes.

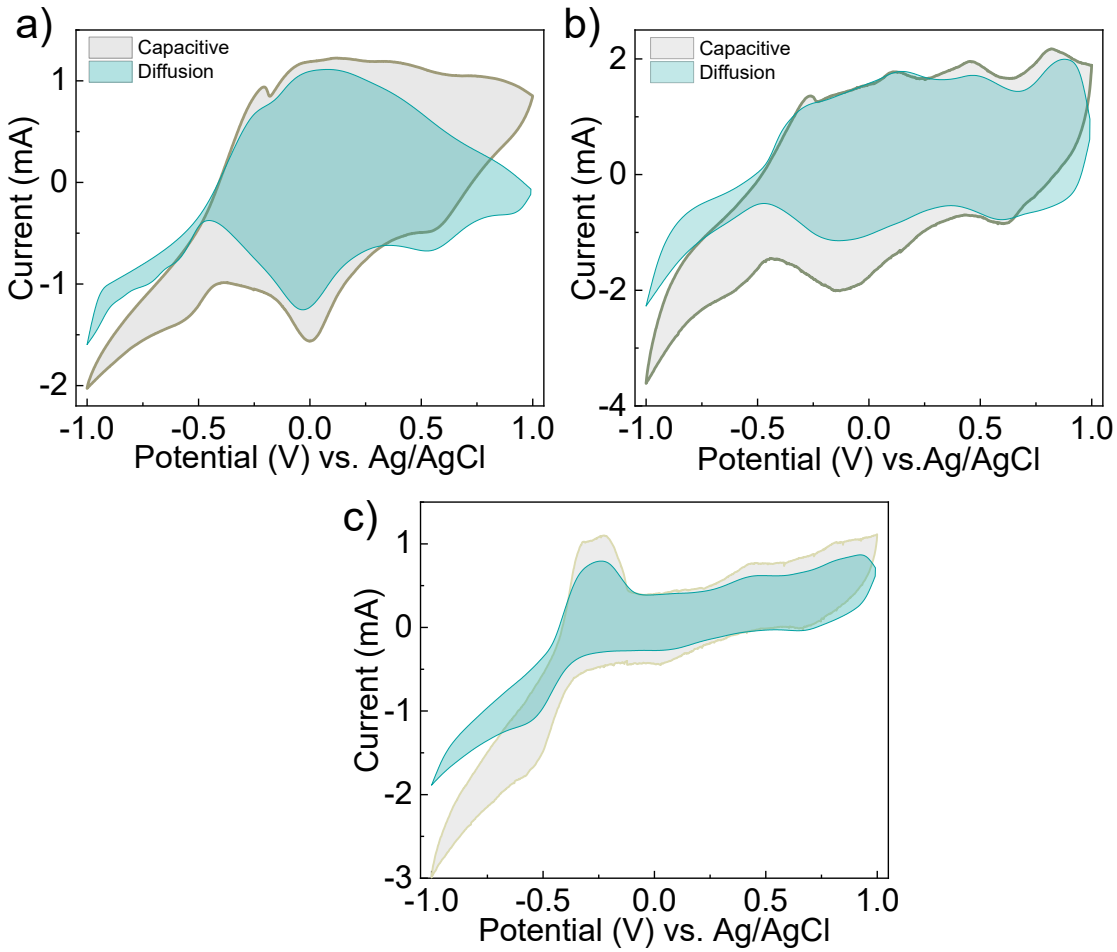

Figure. S6 Capacitive and diffusion-controlled charge storage processes of (a) KVOH-C, (b) 2KVOP-C, and (c) 6KVOP-C, electrodes at 5 mV s^{-1}.

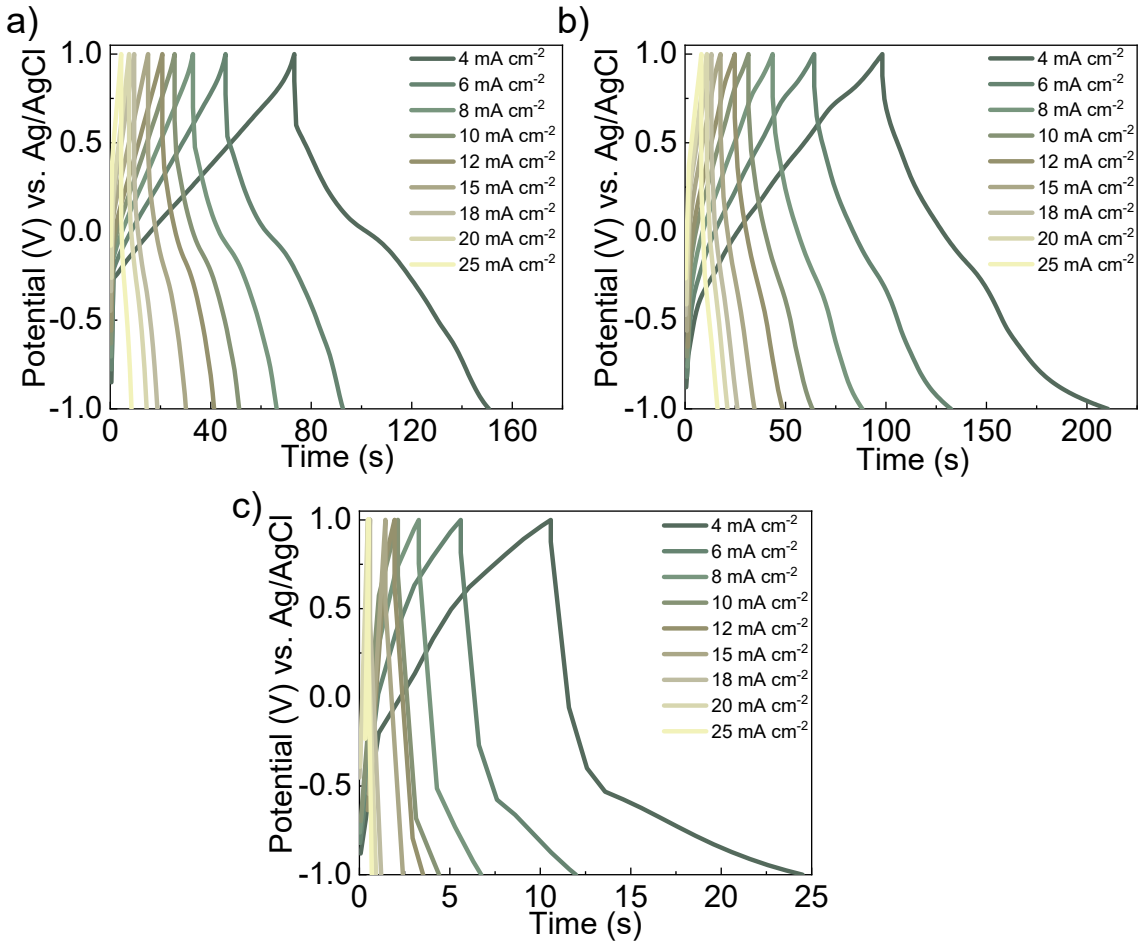

Figure. S7 Galvanostatic charge/discharge curves of (a) KVOH-C, (b) 2KVOP-C, (c) 4KVOP-C, and (d) 6KVOP-C samples for different current densities (4, 6, 8, 10, 12,15, 18, 20, and 25 mA cm^{-2}).

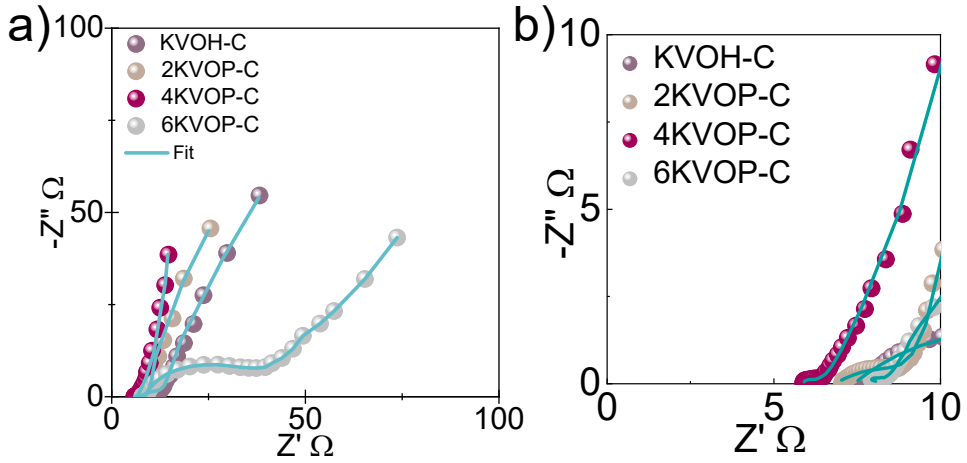

Figure. S8 (a) Nyquist plots with corresponding fitting curves of KVO-C, 2KVOP-C, 4KVOP-C, and 6KVOP-C samples, and (b) enlarged view of the high-frequency region of the Nyquist plots with fitting curves.

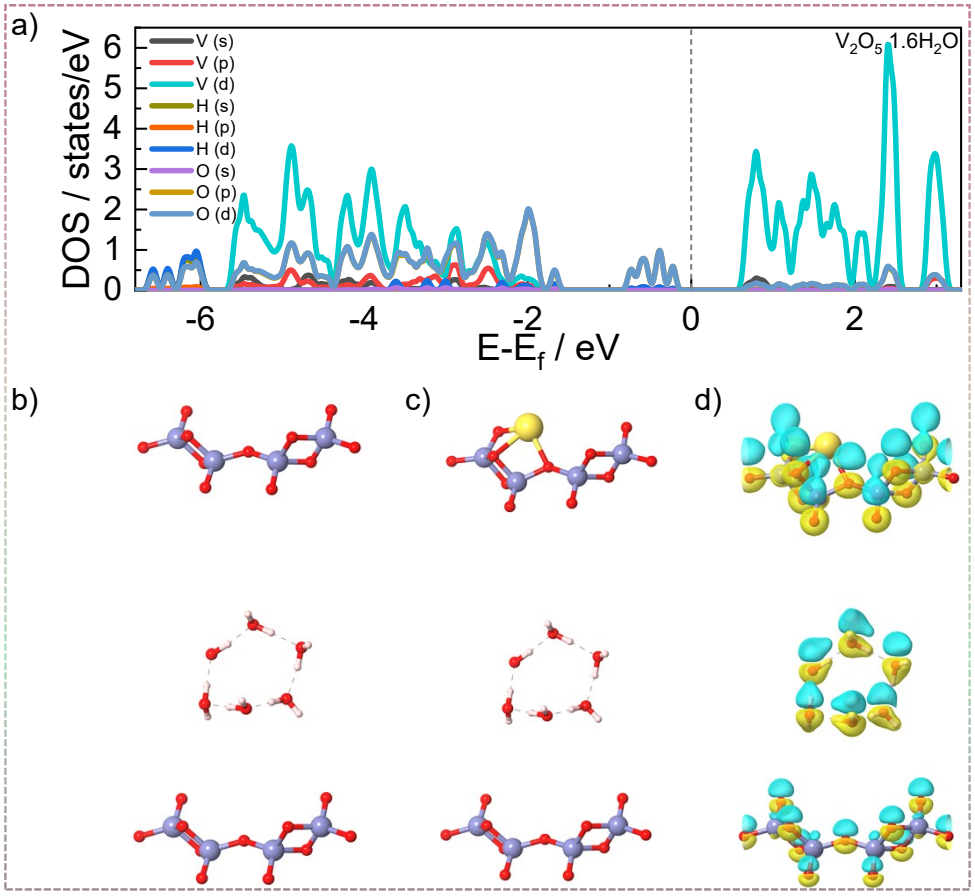

Figure. S9 (a) PDOS of $V_2O_5 \cdot 1.6H_2O$, in which the sparse distribution of near-Fermi electronic states reflects limited intrinsic conductivity. V-3d contributions dominate above E_F , while oxygen-derived states shape the valence-band region; (b, c) Optimized structural configurations showing the geometry of the hydrated vanadium oxide before and after Na adsorption, together with the hydrogen-bonded water ring that stabilizes the interlayer spacing; (d) Corresponding charge-density-difference iso-surfaces for Na adsorption, illustrating the highly localized nature of charge rearrangement within individual VO_6 units, in contrast to the extended charge delocalization observed in the KVOP framework.

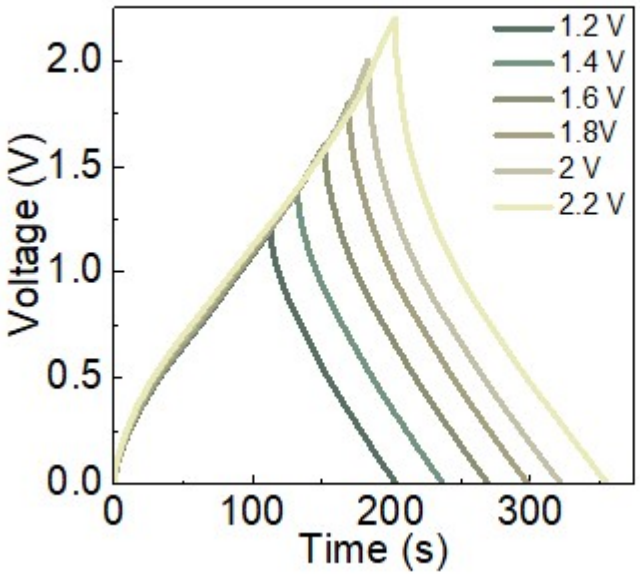

Figure. S10 *Charge/discharge curves of SIS at different voltages from 1.2 to 2.2V.*

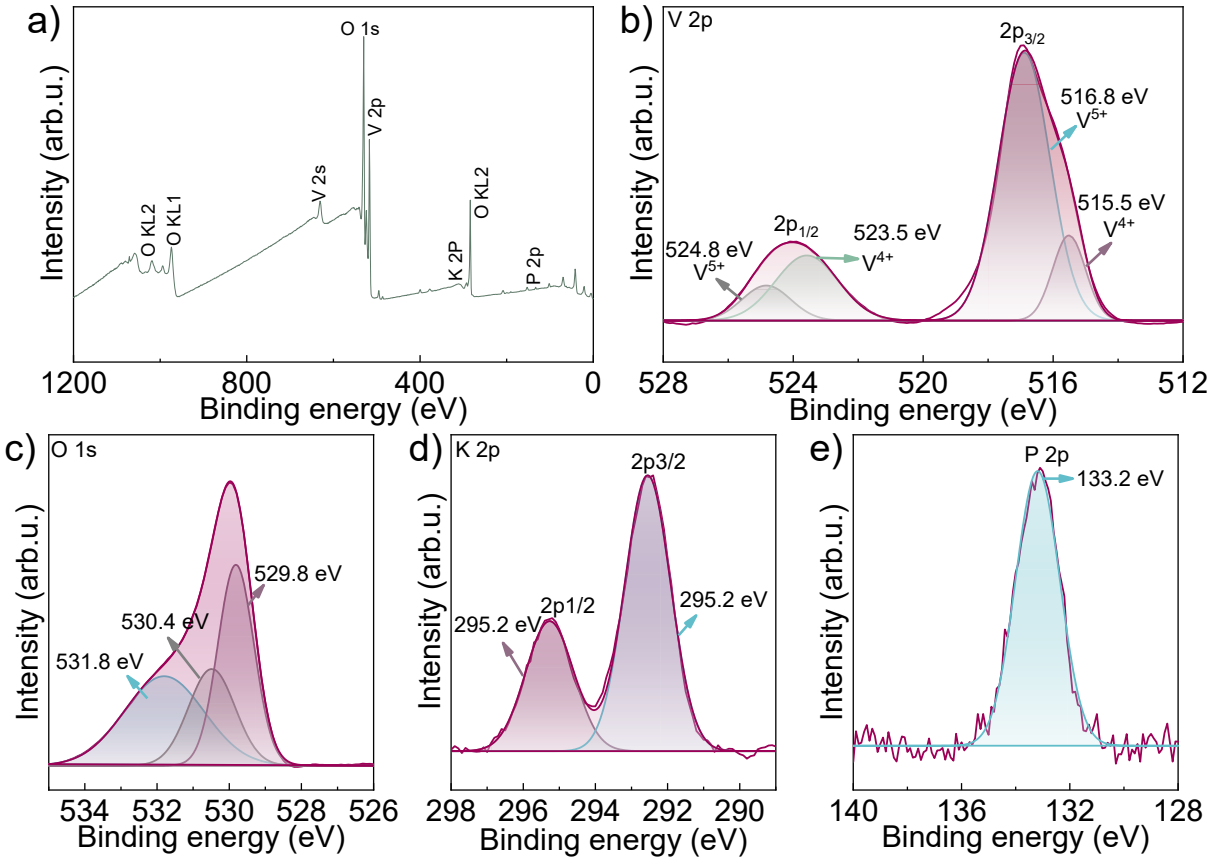

Figure. 11 post-cycling *XPS spectra of the SIS: (a) survey spectrum and high-resolution spectra of (b) V 2p, (c) O 1s, (d) K 2p, and (e) P 2p.*

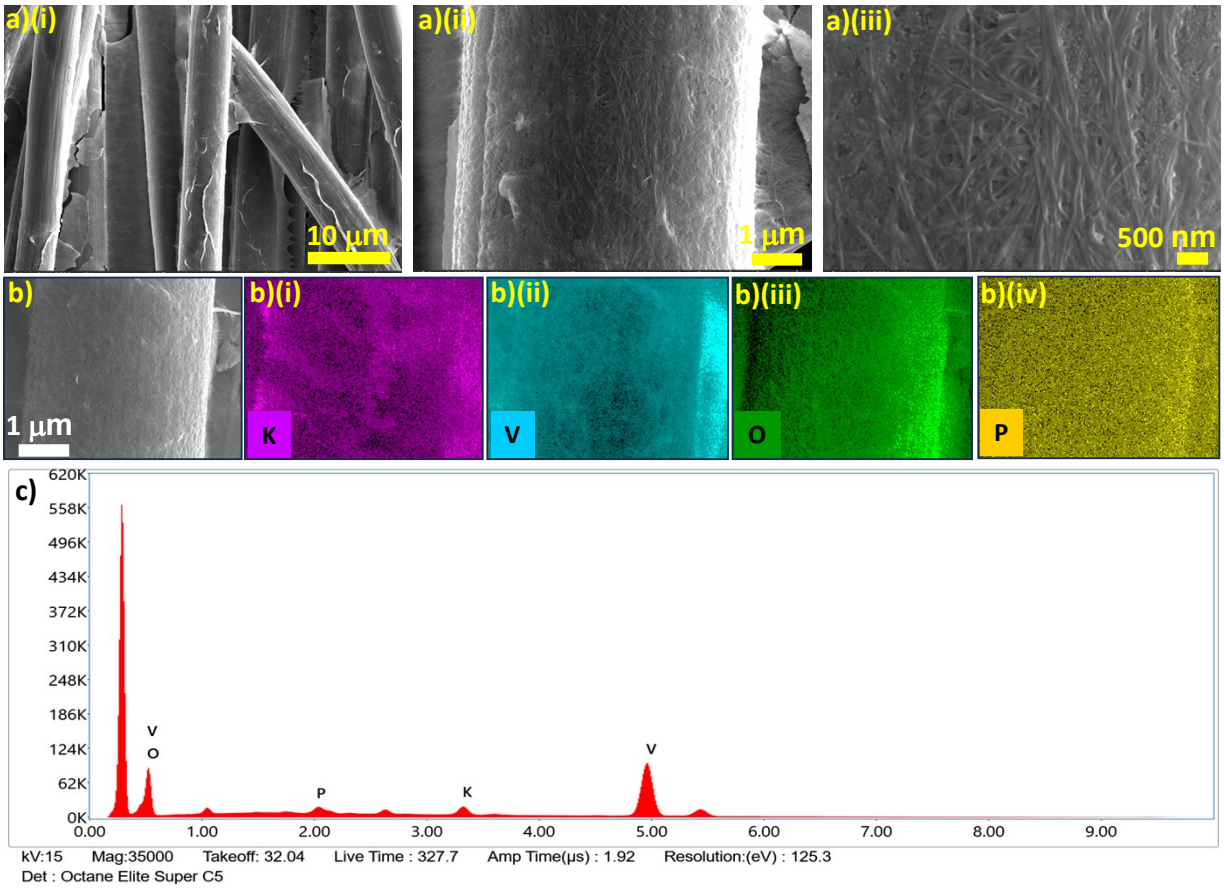

Figure. 12 *(a-c) Post-cycling FE-SEM image, corresponding EDX elemental mapping images, and EDX spectrum.*

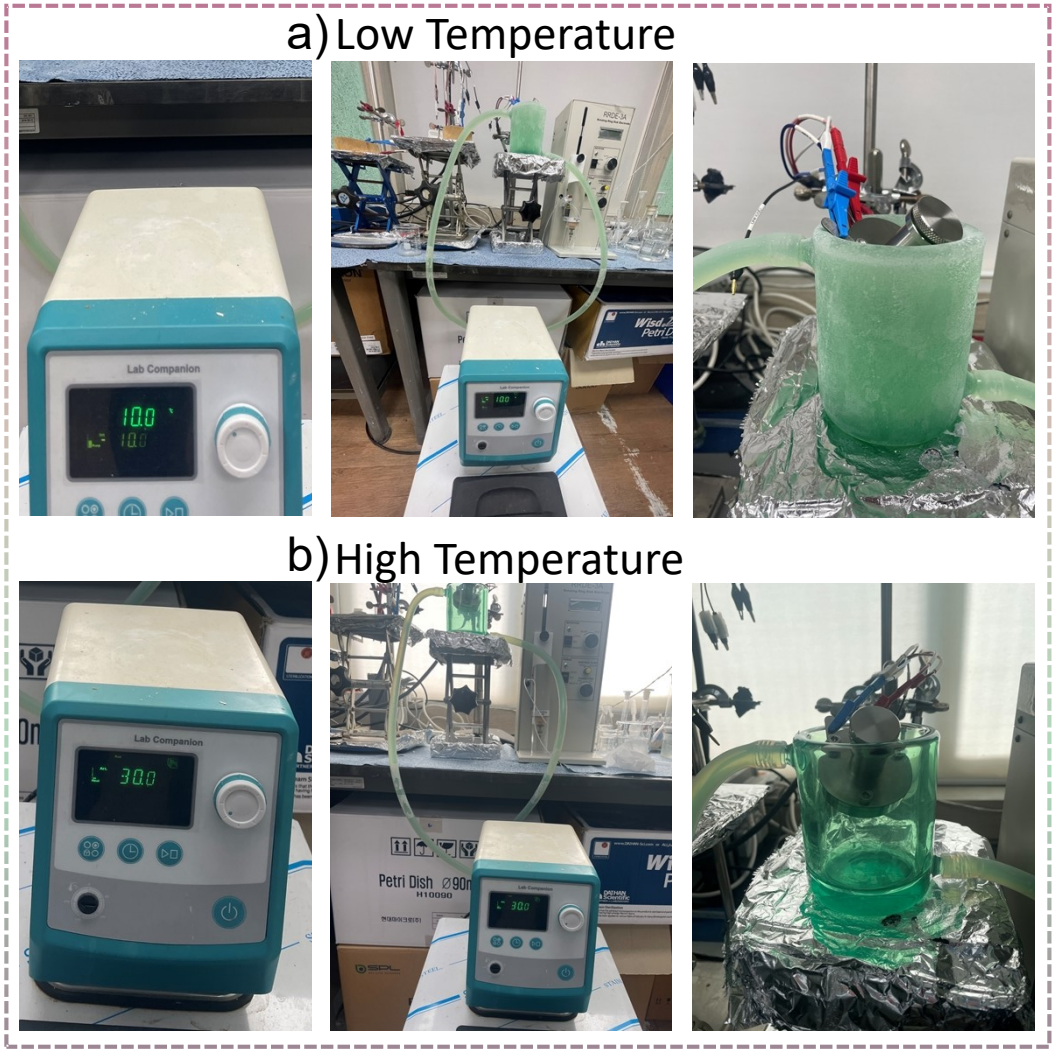

Figure. 13 *photographic images of temperature-dependent electrochemical performance of the SIS measured at (a) 10 ± 1 °C and (b) 30 ± 1°C.*

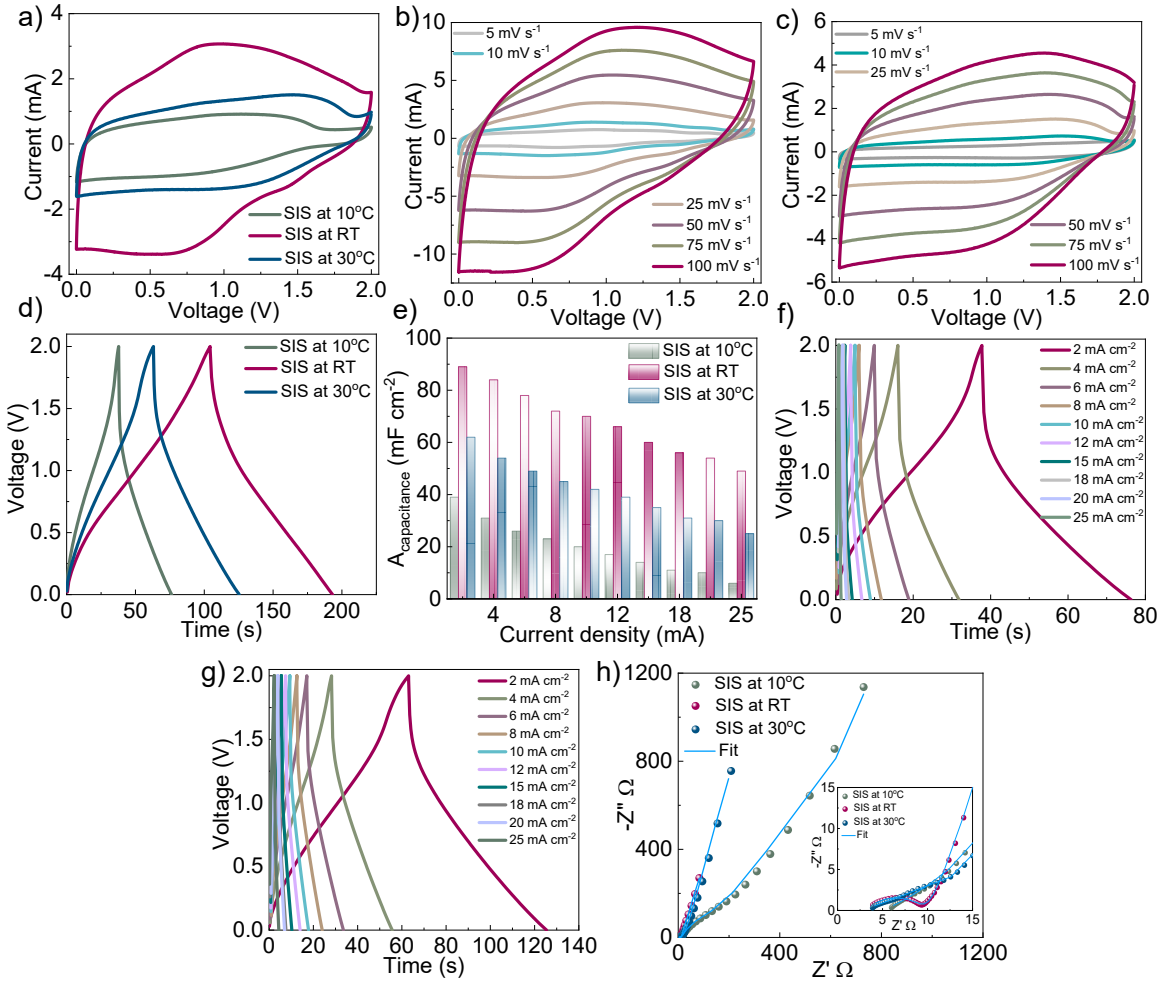

Figure. 14 *temperature-dependent electrochemical performance of the SIS. (a) CV curves of device at different environmental conditions at scan rate of 25 mV s^{-1}, (b and c) CV curves recorded at different scan rates under various temperature conditions, (d) GCD curves of device at different environmental conditions at current density of 2 mA cm^{-2}, (e) comparison of specific capacitance values at varying current densities and temperatures. (f and g) GCD profiles recorded at different current densities under various temperature conditions, and (h) Nyquist plots of the SIS measured under different environmental conditions, with the inset showing the magnified high-frequency region.*

Table S1. EIS fitted parameters of KVOH-C, 2KVOP-C, 4KVOP-C, and 6KVOP-C electrodes, and SIS at different environment.

Parameters	R_s (Ω cm^2)	R_{ct} (Ω cm^2)	W_R (Ω cm^2)	CPE1 (mF cm^{-2})	CPE2 (mF cm^{-2})
KVOH-C	7.4	6.5	10	0.03	0.12
2KVOP-C	6.8	2.1	8.6	0.05	0.15
4KVOP-C	5.8	0.94	6.5	0.35	0.21
6KVOP-C	8.2	19.2	23	0.002	0.032
SIS before stability test	3.35	5.5	0.12	0.06	0.03
SIS after stability test	4.7	6.5	0.42	0.04	0.02
SIS at 10^{o}C	4.6	7.2	23	0.01	0.01
SIS at 30^{o}C	3.5	6.8	12	0.02	0.01

Table S2. Electrochemical performance of present SIS's in comparison with previously reported symmetric supercapacitors.

Samples	Electrolyte	Voltage (V)	Specific energy density (Wh kg^{-1})	Specific power density (W kg^{-1})	Ref.
V_2O_5-Fe_3O_4	3M KOH	0.85	13	1530	1
MCM/V_2O_5-40%	1 M $Al_2(SO_4)_3$	1.6	18	147	2
VP-CC	PVA/$LiClO_4$	1.2	9	199	3
V_3O_7/CFC	[EMIM][OTf]	2	24.7	255	4
Mxene/V_2O_5	1 M Na_2SO_4	1.2	18.4	603	5
V_2O_5-1Mna	PVA-SiO_2-Na_2SO_4 gel	2.2	13.9	1250	6
V_2O_5	1 M $LiClO_4$	1	23.9	937	7
V-Fe-O1@PIECNF	3M KOH	1	24.8	499.9	8
1-MWCNT@SS	0.5 M $NaClO_4$		1.36	-	9
nanoporous V_2O_5	PVA-Na_2SO_3		10.8	-	10
4KVOH-C	Na^+ClO^{4-}/ACN	2	25	990	**This work**

References

1. B. Akkinepally, I. Neelakanta Reddy, C. Lee, T. Jo Ko, P. Srinivasa Rao and J. Shim, *Ceram. Int.*, 2023, **49**, 6280-6288.

2. M. Tian, R. Li, C. Liu, D. Long and G. Cao, *ACS Appl. Mater. Interfaces*, 2019, **11**, 15573-15580.

3. R. Manikandan, C. J. Raj, N. Goli, J.-M. Oh, B. C. Kim, S. Periyasamy and J. Lee, *ACS Appl. Mater. Interfaces*, 2023, **15**, 25452-25461.

4. R. Manikandan, C. J. Raj, M. Rajesh, B. C. Kim, G. Nagaraju, W.-g. Lee and K. H. Yu, *J. Mater. Chem. A*, 2018, **6**, 11390-11404.

5. W. Luo, Y. Sun, Z. Lin, X. Li, Y. Han, J. Ding, T. Li, C. Hou and Y. Ma, *J. Energy Storage*, 2023, **62**, 106807.

6. C. Peng, M. Jin, D. Han, X. Liu and L. Lai, *Mater. Lett.*, 2022, **320**, 132391.

7. S. S. Karade, S. Lalwani, J.-H. Eum and H. Kim, *J. Electroanal. Chem.*, 2020, **864**, 114080.

8. D. Lee, D. Acharya, K. Chhetri, I. Pathak, Y. R. Rosyara, R. M. Bhattarai, T. Kim, T. H. Ko and H. Y. Kim, *J. Energy Storage*, 2025, **112**, 115515.

9. K. S. Morla, T. B. Deshmukh, R. K. Aparna, B. R. Sankapal and A. Banerjee, *Energy Fuels*, 2024, **38**, 21482-21497.

10. R. S. Ingole, S. L. Kadam, N. G. Tiwari, U. T. Nakate, R. Mangiri, S. B. Kulkarni, B. J. Lokhande and J. G. Ok, *Adv. Sustain. Syst.*, 2024, **8**, 2300535.